Rend. Fis. Acc. Lincei (2015) 26:203–209
DOI 10.1007/s12210-014-0353-6

Scaling in damage by electrical resistance measurements: an application to the terracotta statues of the Sacred Mountain of Varallo Renaissance Complex (Italy)

Gianni Niccolini · Oscar Borla · Federico Accornero · Giuseppe Lacidogna · Alberto Carpinteri

Received: 24 September 2014 / Accepted: 26 October 2014 / Published online: 12 November 2014

Abstract This study concerns the assessment of damage by electrical resistance measurements on laboratory mortar specimens and terracotta statues experiencing different stress conditions. The evolution of damage based on changing resistance shows agreement with theoretical predictions of continuum damage mechanics. We show that continuum damage models provide also theoretical support to estimate statues' residual lifetime by correlating in situ electrical resistance measurements with measurements on the laboratory specimens. Damage assessment based on electrical resistance measurements was carried out on three life-size terracotta statues located in Chapel 17 of the Sacred Mountain of Varallo Renaissance Complex (Italy).

Keywords Cultural heritage maintenance · Non-destructive testing · Damage assessment · Electrical measurements · Terracotta statue

1 Introduction

Contemporary civilization considers the conservation of monuments and art works of past centuries for future generations as an essential duty. For example, Italian historic buildings and monuments are exposed to relevant seismic risk or, more generally, to the action of harsh environment which results in accelerated aging and deterioration (Carpinteri et al. 2010, 2013a, 2014).

G. Niccolini · O. Borla · F. Accornero (✉) · G. Lacidogna · A. Carpinteri
Department of Structural, Geotechnical and Building Engineering, Politecnico di Torino, C.so Duca degli Abruzzi 24, 10129 Turin, Italy
e-mail: federico.accornero@polito.it

The latter case is illustrated by Sacro Monte di Varallo, the oldest of the Sacred Mountains in Piedmont and Lombardy (on the UNESCO World Heritage List since 2003) (Fig. 1). Sacro Monte is an extraordinary benchmark for the definition of conservation methods exploiting new technologies. It is indeed made up of 45 Chapels, with similar problems due to the difficult environmental situation, but never identical (Accornero et al. 2012). There are chapels where the floor is below the level of the ground outside (with the effects of damp, similar to those in the cellars of our houses) others above land level, some surrounded by thick vegetation, therefore in the shade, other well exposed and sunny. The interior decorations are made of different materials which react differently to the ambient humidity: wood terracotta, unfired clay, mortar made with chalk and marble dust, etc. In particular, the chapel interiors contain over 800 life-size wooden and multicolored terracotta statues illustrating the life, passion, death and resurrection of Christ (Figs. 2, 3).

Well-reasoned maintenance and intervention programs on the chapel interiors firstly require the use of non-destructive investigation techniques to assess statues' integrity without altering their state of conservation. Quantitatively evaluating the progressive deterioration of materials is a critical issue due to the treacherous nature of damage phenomena that may suddenly degenerate into catastrophic failures (Johansen and Sornette 2000; Sornette et al. 1998; Zapperi et al. 1997). Around 1500, Leonardo da Vinci was already preoccupied with the characterization of fracture by means of mechanical variables (Lemaitre and Chaboche 1985). However, it is only in 1958 when the development of damage mechanics began. In that year, Kachanov (Kachanov 1986) published the first paper devoted to a continuous damage variable directed towards

Fig. 1 Sacro Monte di Varallo (Italy): the Square of Tribunals

Fig. 2 Sacro Monte di Varallo (Italy): Chapel 33, Ecce Homo

Fig. 3 Sacro Monte di Varallo (Italy): Chapel 17, The Transfiguration of Christ on Mount Tabor, a devoted

modeling the deterioration of materials prior to macroscopic fracture.

Electrical resistance measurements and acoustic emission (AE) technique make experimentally accessible the damage variable introduced in damage mechanics (Bridgman 1932; Carpinteri and Lacidogna 2007; Carpinteri et al. 2013b; Chen and Liu 2008; Lacidogna et al. 2011; Niccolini et al. 2011, 2013; Russell and Hoskins 1969). The combined application of these non-destructive investigation techniques has already proved to be a powerful tool for damage assessment in rocks and concrete (Chen and Liu 2008).

In literature research studies investigated the possibility of correlating AE activity in a structure with analogous activity detected on specimens taken from the structure and tested to failure (Carpinteri and Lacidogna 2007; Carpinteri et al. 2013b; Niccolini et al. 2011). Analogously, in the next sections we present in situ and laboratory applications of a simple and inexpensive equipment for electrical resistance measurements. Thus, the evolution of ongoing damage processes in laboratory specimens and terracotta statues is assessed.

2 Damage variable and its electrical resistance change representation

The phenomenon of damage from a physical point of view represents surface discontinuities in the form of microcracks, or volume discontinuities in the form of voids, and it is marked by pronounced irreversibility. It can be very difficult to macroscopically distinguish a highly damaged volume element from a virgin one, since depth of cracks or inner defects cannot be quantified or identified. It, therefore, becomes necessary to imagine internal variables representing the deteriorated state of the material, which are directly accessible to measurements (Lemaitre and Chaboche 1985).

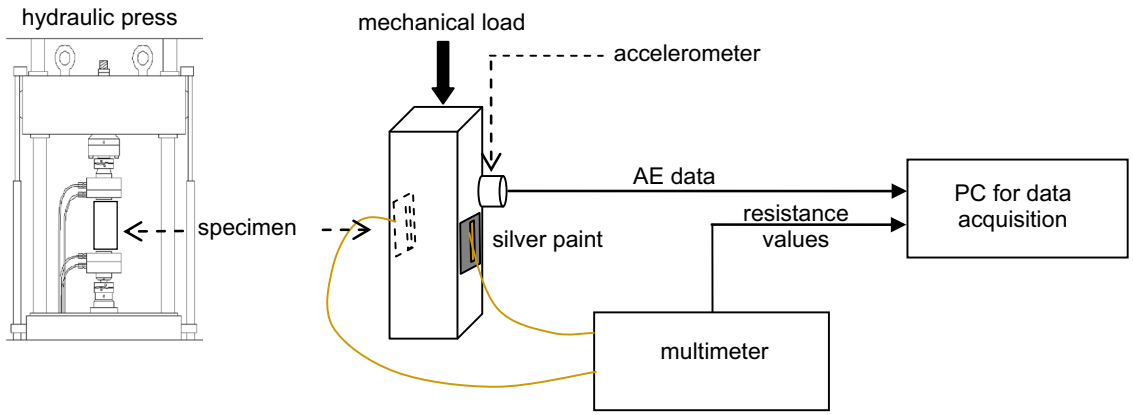

Fig. 4 Schematic representation of the laboratory experimental set-up

A damage variable D can be defined by $D_n = S_0/S$, where S is the cross-sectional area (with normal $\mathbf{n}$) of the considered volume element V and S_0 is the total area of the defect traces (microcracks, voids, etc.) on this section (Kachanov 1986; Krajcinovic 1996; Krajcinovic and Rinaldi 2005; Lemaitre and Chaboche 1985). Considering a distribution of defects without preferred orientation, the damage variable is a scalar quantity: $D_n = D, \forall\, \mathbf{n}$. The damage variable D introduced in damage mechanics quantifies the deviation of a brittle material from linear elasticity, $\sigma = E_0\,(1 - D)\,\varepsilon$, where σ and ε are, respectively, the stress and the strain in the material, and E_0 is the Young modulus of the undamaged material. In general, $0 \leq D \leq 1$. When $D = 0$ linear elasticity is applicable to the material which is still in undamaged state; as $D \to 1$ ($\varepsilon \to \infty$) failure occurs.

In recent years, the correlation of electrical resistance of solids with damage has been investigated as well. As the failure stress is approached, opening of micro- and macrocracks causes more void space in the material and consequently a higher electrical resistance (Bridgman 1932; Russell and Hoskins 1969). Some definitions of damage variable based on electrical resistance changes have been developed (Chen and Liu 2008; Lacidogna et al 2011; Lemaitre and Dufailly 1987; Sun and Guo 2004), the simplest one being

$$D = 1 - R_0/R = (R - R_0)/R. \quad (1)$$

where $R - R_0$ is the increase in electrical resistance between the damaged and the undamaged state. When the material ruptures into two parts ($D \to 1$) the electrical resistance becomes infinite ($R \to \infty$), as consistently stated by Eq. (1).

3 Time-dependent stress on laboratory specimens

A schematic diagram of the equipment used in conducting the experimental study is shown in Fig. 4. We consider two prismatic mortar specimens (Sect. 40 × 40 mm^2, height 160 mm) enriched with iron oxide to increase the electrical conductivity (Niccolini et al. 2013). The chemical analysis results of mortar are shown in Table 1.

Table 1 Chemical composition of mortar enriched with iron oxide

Element	Weight (%)
SiO_2	59.7
CaO	21.4
Fe_2O_3	8.4
Al_2O_3	3.3
SO_3	1.1
K_2O	1.0
MgO	0.7
Na_2O	0.4
Other oxides	4.0

The specimens were subjected to uniaxial compression until failure at constant displacement rate of 2 μm s^{-1}. This condition was applied by a servo-hydraulic press MTS (maximum capacity 500 kN) equipped with control electronics.

Two types of measurements were carried out on the loaded specimens. Electrical resistance measurements were made with the constant voltage method, using an Agilent 34411A multimeter capable of measuring resistances as high as 1 GΩ. Each specimen was connected to the multimeter using two copper electrodes. Prior to testing, the specimen faces on which the electrodes were attached were coated with a conducting silver paint to minimize the contact resistance (Guarino et al. 1998). Initial resistance measurements were, thus, made on both specimens with no stress applied. Very close values ($R_0 = 0.44$ and 0.46 MΩ) were found for the two specimens. Then, the changing resistance R (averaged over 4 s) was measured during loading test until the specimen failed. The resistance at the time of failure was about 12 MΩ for both specimens.

Furthermore, acoustic emission (AE) events associated with microcracks were measured using a calibrated accelerometer mounted on the specimen surface (Carpinteri et al. 2013b; Colombo et al. 2003; Lockner 1993). The sensitivity of the accelerometer is 9.20 pC/m s^{-2}. AE measurement was made over the range of few hertz to 10 kHz at the sampling rate of 44.1 kHz. Prior to testing, the detection threshold was set to filter out spurious noisy signals. Each AE event was characterized by the time of occurrence and the magnitude M, expressed in dB through the relation $M = 20 \log(a_{max}/1\ \mu m\ s^{-2})$, where a_{max} is the peak acceleration on the specimen surface produced by the AE wave.

Figure 5 shows results of the two loading tests. On this figure, the axial compressive stress applied to the specimens, the electrical resistance R, the time series of AE event amplitudes and the accumulated number of AE events are plotted vs. time.

From the stress–time diagrams of Fig. 5, it is observed that linear elasticity is applicable until the failure stress σ_f has been reached. This behavior is referred to as brittle failure. Despite the absence of significant deviations from linear elasticity, the increase in electrical resistance and AE activity during the approach to failure indicates that damage is accumulating within the specimens.

We consider the dependence of the electrical resistance R on the non-dimensional stress σ/σ_f. A reasonably simple function fitting to the experimental data is a scaling law

$$R(x) = \frac{\beta}{(1-x)^{\alpha}}, \tag{2}$$

where $x \equiv \sigma/\sigma_f$ is the normalized stress. The fit yields $\alpha = 0.35 \pm 0.07$, and $\beta = 0.39 \pm 0.09$. In the limit $x \to 0$, there results $R(0) = \beta$, which is statistically indistinguishable from the initial values R_0 observed experimentally.

Now compare the results derived above with damage mechanics model. Looking again at the stress–time diagrams of Fig. 5, we can assume that the applied stress σ is increased linearly with time

$$\sigma(t) = Ct, \tag{3}$$

where C is a constant. Substitution of Eq. (3) into Eq. (2) gives

$$R(t) = \frac{\beta}{\left(1 - \frac{t}{t_f}\right)^{\alpha}}, \tag{4}$$

where $t_f = \sigma_f/C$ is the time of failure. The time evolution $R(t)$ of the electrical resistance is shown in Fig. 6a.

Combining Eqs. (1) and (4), we find power-law scaling of the damage variable D during the approach to failure

$$D(t) = 1 - \frac{R_0}{\beta}\left(1 - \frac{t}{t_f}\right)^{\alpha}. \tag{5}$$

The scaling observed in our experiments is the same as that predicted by damage mechanics in the case of linearly

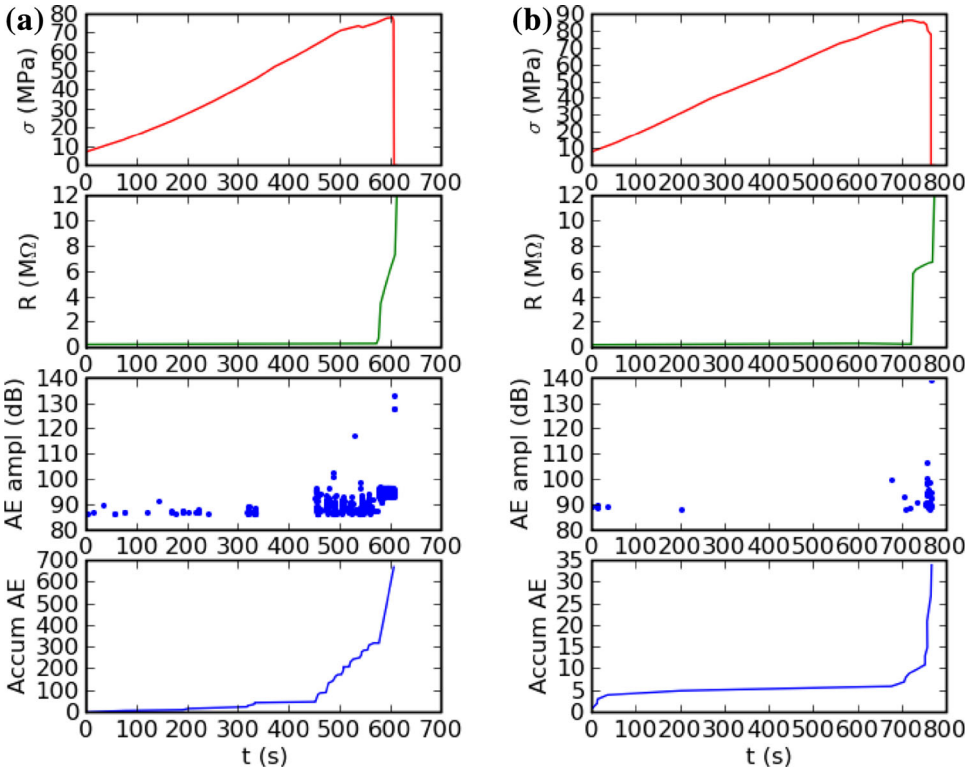

Fig. 5 Applied stress, electrical resistance, AE event amplitudes and cumulative AE event number vs. time for mortar specimens (**a**, **b**)

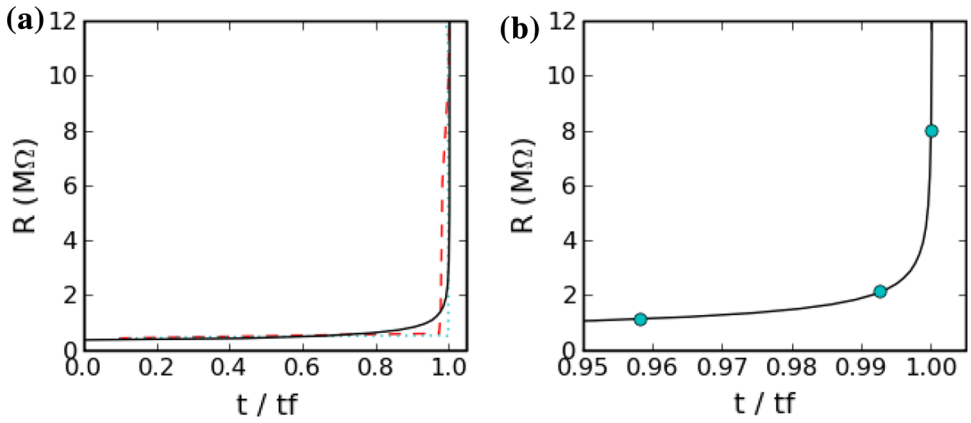

Fig. 6 **a** Electrical resistance as a function of time to failure t/t_f: *dashed* and *dotted lines* represent experimental data from laboratory specimens, while continuous line represents the fitting function given by Eq. (4). **b** Detail *circles* identifying the time to failure t/t_f of the three statues

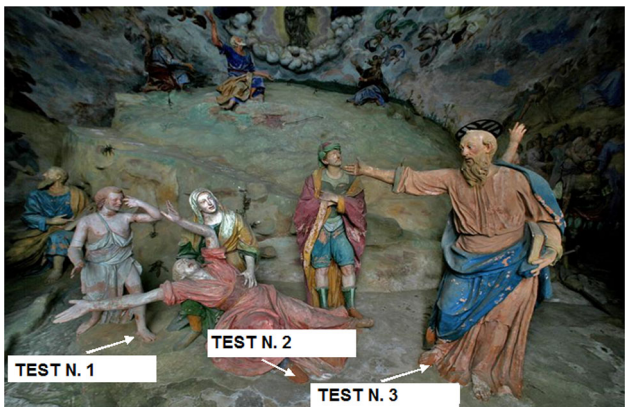

Fig. 7 Sacro Monte di Varallo (Italy): Chapel 17, The Transfiguration of Christ on Mount Tabor *Labels* indicate the monitored portions of terracotta statues

time-dependent stress (Turcotte et al. 2002; Turcotte and Shcherbakov 2003):

$$D(t) = 1 - \left(1 - \frac{t}{t_f}\right)^{1/3}. \quad (6)$$

More specifically, the values of parameters α, β and R_0 make the experimental fitting function defined by Eq. (5) statistically indistinguishable from the theoretical function defined by Eq. (6). This result is in agreement also with the power-law behavior of cumulative energy associated with acoustic emission events prior to the failure of circular panels of chipboard and fiberglass (Guarino et al. 1998).

4 Constant stress on terracotta statues

In situ damage assessment based on electrical resistance measurements was carried out on three life-size terracotta statues located in the Chapel 17 of the Sacred Mountain of Varallo in Italy (Fig. 1), This Chapel houses the scene of the Transfiguration of Christ on Mount Tabor (Fig. 7). The statues present hollows on their hidden sides, appearing polished only on those parts exposed to the gaze of the viewer. They could be at risk of collapse due to the action of harsh environment, including ambient humidity, dust, organic deposits, etc. (Accornero et al. 2012). The resistance was measured on the statues' ankles, which are weak spots due to their small cross sections. At the ankle level, the effective load-carrying area element is an annulus of about 30 cm^2. Measured resistances averaged 1.18, 2.16 and 8 MΩ, for the three statues, respectively.

Table 2 Chemical composition of historical terracotta

Element	Weight (%)
SiO_2	51.9
Al_2O_3	16.0
CaO	12.9
Fe_2O_3	10.3
Other oxides	8.9

The chemical composition of historical terracotta, as shown in Table 2, is remarkably close to those of mortar previously identified.

In the laboratory analysis, we considered the case in which the applied stress was a linearly increasing function of time. Now, we can assume that a constant axial stress σ_0 is applied to the statues' ankles due to dead load.

Generally, if $\sigma_0 \leq \sigma_y$, where σ_y is the yield stress, the material obeys linear elasticity and no damage occurs. If a stress $\sigma_0 > \sigma_y$ is applied and maintained, the material fails in a finite time (Turcotte et al. 2002; Turcotte and Shcherbakov 2003). The signs of aging and deterioration shown by the statues suggest that stress may exceed the yield limit, especially in the weaker spots.

The close similarity between terracotta ankles and mortar specimens in chemical composition and size suggests analogous electrical properties. Then, it seems reasonable that the electrical resistance of terracotta ankles and mortar specimens could be the same for the particular

stress level reached. Furthermore, it has been demonstrated (Turcotte and Shcherbakov 2003) that the dependence of the damage variable D on the time to failure t/t_f,when the applied stress is constant, is given by the same power-law behavior in Eq. (6) for stress increasing linearly with time.

Thus, we can argue that the points specifying the state of the three statues lie on the lifetime curve of mortar specimens. This scaling approach to failure is illustrated in Fig. 6b. The predicted values of time to failure t/t_f using Eq. (4) are 0.957, 0.992 and 0.999 for the three statues, being $t = 340$ years their age (the last dates back to the 1670s). The residual lifetime of the statues is then estimated, in terms of time $t_f - t$ before the maximum value of electrical resistance is reached in the analyzed elements, at 15, 2.5 and 0.1 years.

Finally, at least one statue seems to require urgent restoration intervention. The application of geopolymer restoration techniques (Hanzlicek et al. 2009) to the unseen part of the statues, ensuring stability and durability without disrupting the esthetics, may be strongly recommended.

5 Conclusions

The damage assessment by means of electrical resistance testing shows agreement with theoretical predictions of continuum damage mechanics. We consider two cases: (1) the load applied to mortar specimens increases linearly with time from zero until failure and (2) a constant compressive load applied to terracotta statues belonging to Chapel 17 of the Sacred Mountain of Varallo Renaissance Complex (Italy). (Turcotte et al. 2002; Turcotte and Shcherbakov 2003) theoretically approached the failure of solids using continuum damage mechanics models. They found that the cumulative damage under has a power-law dependence on the time to failure with identical power-law exponent $\alpha = 1/3$ for loading conditions (1) and (2). We have shown that this dependence is in agreement with the solutions obtained in our laboratory experiments using electrical resistance measurements. Furthermore, identical solutions for cases (1) and (2) provide the theoretical support to estimate terracotta statues' residual lifetime by correlating in situ electrical measurements with laboratory measurements.

Thus, the presented methodology should have properly illustrated the need for damaged artworks and more in general for cultural heritage to have a planned preventative maintenance.

References

Accornero F, Invernizzi S, Lacidogna G, Carpinteri A (2012) Acoustic Emission and damage analysis of decorated surface structural supports. In: Proceedings of the 19th European conference on fracture (ECF19), Kazan, Russia

Bridgman PW (1932) The effect of homogeneous mechanical stress on the electrical resistance of crystals. Phys Rev 42:858

Carpinteri A, Lacidogna G (2007) Damage evaluation of three masonry towers by acoustic emission. Eng Struct 29:1569

Carpinteri A, Invernizzi S, Lacidogna G, Manuello A (2010) Preservation, safeguard and valorization of masonry decorations in the architectural historical heritage of Piedmont (Italy). Adv Mater Res 133–134:1015–1020

Carpinteri A, Lacidogna G, Invernizzi S, Accornero F (2013a) The Sacred Mountain of Varallo in Italy: seismic Risk Assessment by Acoustic Emission and Structural Numerical Models. Sci World J 2013:170291

Carpinteri A, Lacidogna G, Accornero F, Mpalaskas AC, Matikas TE, Aggelis DG (2013b) Influence of damage in the acoustic emission parameters. Cement Concr Compos 44:9–16

Carpinteri A, Lacidogna G, Accornero F (2014) Evolution of the fracturing process in masonry arches. J Struct Eng ASCE. doi:10.1061/(ASCE)ST.1943-541X.0001071

Chen B, Liu J (2008) Damage in carbon fiber-reinforced concrete, monitored by both electrical resistance measurement and acoustic emission analysis. Constr Build Mater 22:2196

Colombo S, Main IG, Forde MC (2003) Assessing damage of reinforced concrete beam using "b-value" analysis of acoustic emission signals. J Mater Civ Eng ASCE 15:280

Guarino A, Garcimartin A, Ciliberto S (1998) An experimental test of the critical behavior of fracture precursors. Eur Phys J B 6:13

Hanzlicek T, Steinerova M, Straka P, Perna I, Siegl P, Svarcova T (2009) Reinforcement of the terracotta sculpture by geopolymer composite. Mater Des 30:3229

Johansen A, Sornette D (2000) Critical ruptures. Eur Phys J B 18:163

Kachanov LM (1986) Introduction to continuum damage mechanics. Martinus Nijhoff, Dordrecht

Krajcinovic D (1996) Damage mechanics. Elsevier, Amsterdam

Krajcinovic D, Rinaldi A (2005) "Statistical damage mechanics", 2005 *Trans*. ASME 72:76

Lacidogna G, Carpinteri A, Manuello A, Niccolini G, Agosto A, Borla O (2011) Acoustic emission and electrical properties of quasi-brittle materials under compression. In: Proceedings of conference & exposition on experimental and applied mechanics (SEM), Uncasville, CT, USA

Lemaitre J, Chaboche J (1985) Mechaniques des materiaux solides. Dunod, Paris

Lemaitre J, Dufailly J (1987) Damage measurements. Eng Fract Mech 28:643

Lockner D (1993) The role of acoustic emissions in the study of rock fracture. Int J Rock Mech Min Sci Geomech Abstr 7:883

Niccolini G, Carpinteri A, Lacidogna G, Manuello A (2011) Acoustic emission monitoring of the Syracuse Athena temple: scale invariance in the timing of ruptures. Phys Rev Lett 106:108503

Niccolini G, Borla O, Accornero F, Lacidogna G, Carpinteri A (2013) Mechanical damage of historical terracotta statues analyzed by electrical resistance measurements. In: Proceedings of the 21st congress of the Italian society of theoretical and applied mechanics (AIMETA XXI), Turin, Italy

Russell JE, Hoskins ER (1969) Correlation of electrical resistivity of dry rock with cumulative damage. In: Proceedings of the 11th US symposium on rock mechanics, American Rock Mechanics Association, Berkeley

Sornette D, Leung KT, Andersen JV (1998) Conditions for abrupt failure in the democratic fiber bundle model. Phys Rev Lett 80:3158

Sun B, Guo Y (2004) High-cycle fatigue damage measurement based on electrical resistance change considering variable electrical resistivity and uneven damage. Int J Fatigue 26:457

Turcotte DL, Shcherbakov R (2003) Damage and self-similarity in fracture. Theoret Appl Fract Mech 39:245

Turcotte DL, Newman WI, Shcherbakov R (2002) Micro and macroscopic model for rock fracture. Geophys J Int 152:718

Zapperi S, Ray P, Stanley HE, Vespignani A (1997) First-order transition in the breakdown of disordered media. Phys Rev Lett 78:1408